J Mater Sci (2011) 46:275–284
DOI 10.1007/s10853-010-4982-6

One-step and iterative thermo-mechanical treatments to enhance $\Sigma 3^n$ boundaries in a Ti-modified austenitic stainless steel

Sumantra Mandal · A. K. Bhaduri · V. Subramanya Sarma

Received: 11 June 2010 / Accepted: 5 October 2010 / Published online: 22 October 2010

Abstract The article discusses the results of a study on low-strain thermo-mechanical (one-step and iterative) processing to enhance $\Sigma 3^n$ boundaries in a Ti-modified austenitic stainless steel (alloy D9). Solution annealed (SA) specimens were subjected to 10% thickness reduction by rolling followed by annealing at 1173, 1223, and 1273 K for 0.5, 1, and 2 h. Anomalous grain growth with moderate increase in $\Sigma 3^n$ boundaries was observed after annealing at 1,173 K for 0.5 to 2 h. Prolific multiple twinning with minimum deviation of $\Sigma 3$ and $\Sigma 9$ boundaries from ideal orientation was achieved after annealing at 1,273 K for 0.5 to 2 h. A significant disruption in random boundary connectivity was obtained in these conditions due to the presence of large number of $\Sigma 3$-$\Sigma 3$-$\Sigma 9$/$\Sigma 3$-$\Sigma 9$-$\Sigma 27$ triple junctions. Iterative processing (up to 4 cycles) employing 10% thickness reduction followed by annealing at 1,273 K for 0.5 h revealed fluctuations in the evolution of $\Sigma 3$ boundaries. The $\Sigma 3$ fraction increased after 2nd and 4th iteration and there is a drop after 3rd iteration. This was attributed to the increased driving force for grain boundary migration due to dislocation pile-up at twin boundaries during earlier iterations. A two step iterative processing comprising of 10% deformation followed by annealing at 1,273 K for 0.5 h is the recommended thermo-mechanical processing to achieve enhanced fraction of $\Sigma 3^n$ boundaries ($\sim$73%) in alloy D9.

S. Mandal (✉) · A. K. Bhaduri
Materials Technology Division, Indira Gandhi Centre for Atomic Research, Kalpakkam 603102, India
e-mail: sumantra@igcar.gov.in

S. Mandal · V. Subramanya Sarma
Department of Metallurgical and Materials Engineering, Indian Institute of Technology Madras, Chennai 600036, India

V. Subramanya Sarma
Department of Materials Science and Engineering, North Carolina State University, Raleigh, NC 27695-7919, USA

Introduction

It is well established that the physical, chemical, and mechanical properties of polycrystalline materials are controlled by the number as well as the structure of grain boundaries. The concept of "grain boundary design and control" (by exploiting certain type of grain boundaries for their beneficial properties) was first introduced by Watanabe [1], and the topic has evolved into "grain boundary engineering" (GBE). Essentially, GBE implies manipulation of the grain boundary character distribution (GBCD) to improve bulk polycrystalline properties. The main focus of GBE is to optimize the GBCD by increasing the proportion of special boundaries (SBs), since these show increased resistance to segregation [2], intergranular cracking [3], embrittlement [4], corrosion [5–8], creep [9], fatigue [10], and fracture [11, 12].

The so called SBs have a lower energy and contribute to the improvement in properties due to their closer atomic packing in comparison to the random high-angle boundaries (HABs) and are often described in terms of coincidence site lattice (CSL) model. Though it was initially believed that all CSL boundaries are "special", recent results show that only a subset of CSLs are special [7, 13]. A recent and more complete description of special boundary is the one which terminates on low index planes [14]. In practice, GBE has been extensively applied to low stacking fault energy (SFE) materials as they exhibit prolific twinning during annealing and every CSL boundary in

GBE microstructure in low SFE materials is essentially a $\Sigma 3^n$ ($n = 1, 2, 3$) boundary with annealing twins being a subset of $\Sigma 3$ CSL boundaries [15]. Since, $\Sigma 3$ boundaries are generally associated with special properties; research is focused on increasing the fraction of $\Sigma 3$ boundaries through twinning-related GBE [16]. The higher order twin boundaries (i.e., $\Sigma 9$ and $\Sigma 27$) may not always terminate on the low index plane and whether or not they are "special" depends on their terminating on the low index plane [17]. However, the main role of $\Sigma 9$ and $\Sigma 27$ boundaries in GBE is rather geometric; they take part in the reconfiguration of the existing grain boundary network that eventually breaks down the random HABs connectivity.

The methodology to manipulate grain boundaries is through thermo-mechanical processing (TMP), i.e., through prior deformation and annealing. There are no fixed process route/parameters to achieve optimum GBE microstructure in all materials. This could be attributed to the number of variables associated with the processing, such as the material properties (especially SFE), the starting microstructure, the mode (tension, compression or rolling) and amount of strain employed, the annealing time and temperature, and the number of deformation-annealing iterations employed [18]. Iterative thermo-mechanical processing (ITMP) involving several cycles of strain-recrystallization or strain-annealing treatment is usually employed to obtain a GBE microstructure [19–21]. Iterative strain-recrystallization processing involves medium to high levels of strain (typically 20–30%) followed by a short annealing for a few minutes at a temperature of 0.6–0.8 T_m. Iterative strain annealing, on the other hand, involves small amount of strain (typically <7%) followed by annealing for many hours at temperatures below recrystallization [22]. Some recent studies on austenitic stainless steels (304 and 316) have also reported very high fractions of $\Sigma 3^n$ achieved through one-step thermo-mechanical processing (OTMP) route [23, 24]. These OTMP is based on very low ($\sim$3–6%) level of deformation followed by annealing at high temperature (1,173–1,240 K) for very long duration (72–96 h). Though these OTMP routes can be readily implemented in industry when compared to ITMP, the longer annealing time would decrease production rate and increase production cost. Annealing for long time at high temperatures can also result in significant grain growth and this will have detrimental effect on mechanical properties. Further, recent results seem to indicate that in addition to GBCD, grain size also plays crucial role in determining the sensitization resistance of materials [25, 26]. Therefore, in addition to increasing the fraction of $\Sigma 3^n$, grain growth should be minimized to the extent possible during low-strain TMP.

From the above discussion, it is clear that efforts should be made to develop low-strain TMP routes through which GBE microstructure could be realized employing relatively shorter annealing time to minimize grain growth. Recent studies have attempted to establish low-strain TMP routes for GBE with minimum grain growth [27, 28]. However, the underlying mechanism of GBE microstructure development through low-strain processing is not clearly established. The objective of the present study is two-fold. The first objective is to establish a low-strain TMP route to promote $\Sigma 3^n$ boundaries without inducing significant grain growth in a Ti-modified austenitic stainless steel (alloy D9) to prevent/reduce radiation induced segregation. The second objective is to understand the micro-mechanisms involved in the low-strain GBE processing.

Experimental

The chemical composition of alloy D9 used in the present investigation is given in Table 1. Solution annealed (SA) specimens were subjected to 10% thickness reduction in a laboratory rolling mill. Deformed specimens were annealed at three different temperatures (1173, 1223, and 1273 K) for three different durations (0.5, 1, and 2 h) and subsequently quenched in water (WQ). It may be noted here that the extent of pre-strain is an important variable and would have significant effect on GBCD. However, the extent of pre-strain was kept at 10% since the objective of the present study is to develop a low-strain TMP route. The extent of pre-strain below 10% was found to have only a moderate influence on GBCD of alloy D9 [29]. The annealing time is kept short to avoid significant grain growth. Table 2 summarizes the combinations of OTMP conditions adopted in the present study. The SA sample was also subjected to iterative rolling followed by annealing for 1–4 cycles. In each processing cycle, rolling with a thickness reduction of 10% was carried out at ambient temperature, and the subsequent annealing was performed at 1,273 K for 0.5 h. The corresponding specimens for iterative processing were named as G, GG, GGG,

Table 1 Chemical composition (in wt.%) of 15Cr–15Ni–2.2Mo–Ti-modified austenitic stainless steel (alloy D9)

C	Mn	Si	S	P	Cr	Ni	Mo	Ti	Co	N	Fe
0.05	1.51	0.51	0.002	0.01	15.05	15.07	2.25	0.21	0.01	0.006	Bal.

Table 2 One-step thermo-mechanical processing schedules adopted in the present study

Specimen no. SA	Processing conditions Solution annealed
A	10% cold rolled + 1,173 K for 0.5 h + WQ
B	10% cold rolled + 1,173 K for 1 h + WQ
C	10% cold rolled + 1,173 K for 2 h + WQ
D	10% cold rolled + 1,223 K for 0.5 h + WQ
E	10% cold rolled + 1,223 K for 1 h + WQ
F	10% cold rolled + 1,223 K for 2 h + WQ
G	10% cold rolled + 1,273 K for 0.5 h + WQ
H	10% cold rolled + 1,273 K for 1 h + WQ
I	10% cold rolled + 1,273 K for 2 h + WQ

Table 3 Iterative thermo-mechanical processing schedules adopted in the present study

Specimen no.	Processing conditions	Iteration
G	10% cold rolled + 1,273 K for 0.5 h + WQ	1
GG	10% cold rolled + 1,273 K for 0.5 h + WQ	2
GGG	10% cold rolled + 1,273 K for 0.5 h + WQ	3
GGGG	10% cold rolled + 1,273 K for 0.5 h + WQ	4

and GGGG, respectively. Table 3 summarizes the ITMP schedules adopted in the present study.

Electron back scatter diffraction (EBSD)-based orientation imaging microscopy (OIM) scans were performed on all the processed samples to determine the GBCD in the materials using a TSL-OIM system attached to FEI Quanta 200 scanning electron microscope (SEM) operating at 30 kV. OIM maps were collected from the samples using a step size of 1 μm. The grain boundary character is classified as: low angle or Σ1 boundaries are those with misorientation (θ) $5° < \theta \leq 15°$ and boundaries with $2° < \theta \leq 5°$ misorientation are considered as sub-boundaries. To identify CSL boundaries, Brandon's criterion [30] is used. Random HABs are defined as those with misorientation $\theta > 15°$ and which are not low Σ ($\Sigma \leq 29$) CSL boundaries. The grain size was measured using linear intercept method (average of horizontal and vertical intercept lengths) and a misorientation of 5° was used for determining the grain size. To ensure statistical significance, GBCD and average grain size in each sample is analyzed from at least two different maps of 500 × 500 μm^2 areas. The data reported in this article is the average value obtained from at least two maps. The GBCD data is found to vary within ±1%, while the average grain size is found to vary within ±3 μm.

Results

The microstructure revealed by grain boundary OIM map of the SA specimen is shown in Fig. 1. It consists of equiaxed grains while the grain size distribution is marginally inhomogeneous. The SA material contained ~45% of Σ3 boundaries. The proportion of Σ9 and Σ27 boundaries are 2.9 and 0.8%, respectively. A closer look at Fig. 1 reveals that majority of the twin boundaries are not part of the grain boundary network, i.e., they are mainly "neutral" twins. As a result, random HABs are well connected in this specimen and hence provide a potential path for percolation.

Figure 2a shows the microstructural evolution in sample B, which is also the representative microstructure for samples A, C, and D (see Table 2 for sample details). It is observed that anomalous grain growth has taken place in these processing conditions, resulting in a bimodal grain size distribution consisting of large and small grains. The enclosed areas in this sample (regions marked as X and Y in Fig. 2a) highlight the appearance of Σ3 boundaries. It is seen that the morphology of majority of Σ3 boundaries in the bigger grains (i.e., in region X) are straight and parallel, while in the smaller grains (i.e., in region Y) they are predominantly curvilinear. In both the regions, majority of Σ3 boundaries do not take part in the grain boundary network and thereby remain as "non-incorporated" or "neutral" twins in the microstructure. A propensity towards

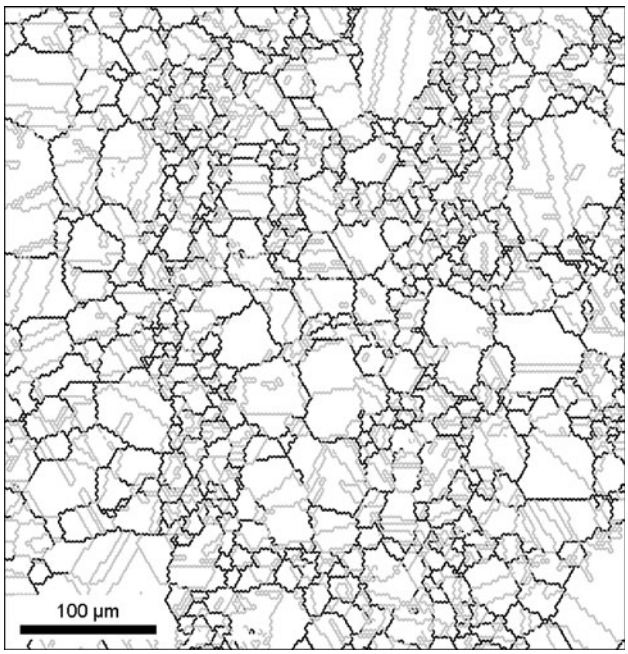

Fig. 1 Grain boundary microstructure of the solution annealed (SA) sample, the *thick black* and *thin gray lines* represent random high-angle boundaries (HABs) and low Σ CSL boundaries, respectively

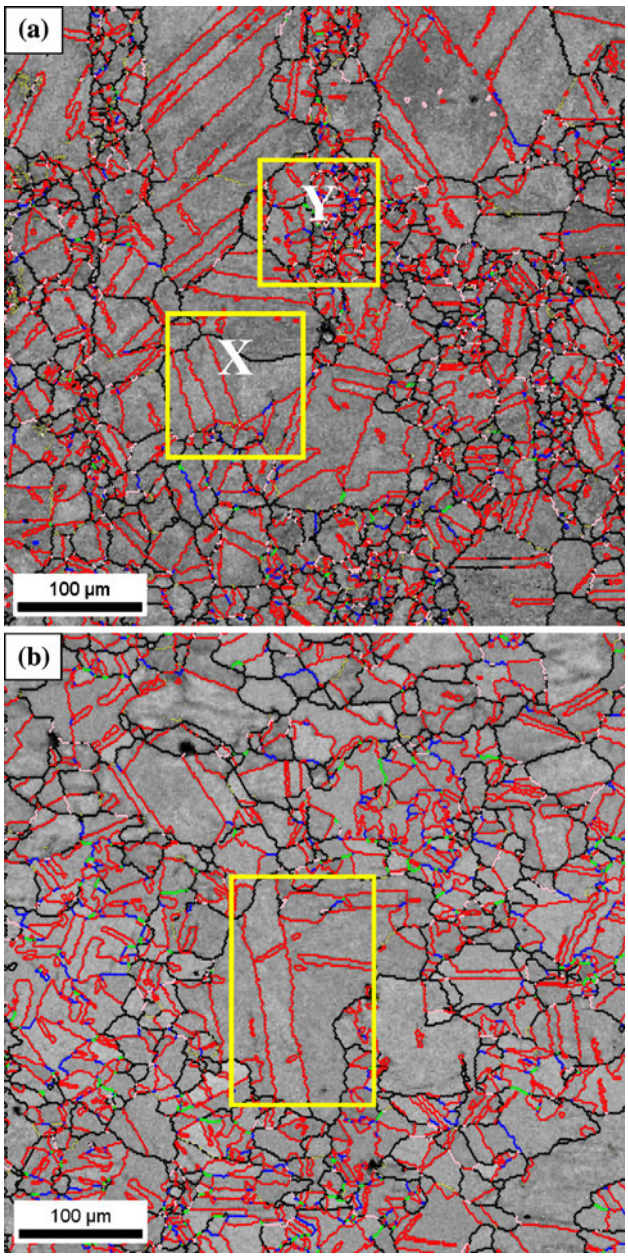

Fig. 2 Image quality (IQ) map (color code for the grain boundaries: Σ3—*red*; Σ9—*blue*; Σ27—*green*; other low Σ CSL—*purple*, random HABs—*black*) of samples **a** B; and **b** E (see Table 2 for sample description) (Color figure online)

homogeneous grain size distribution is observed in sample E (Fig. 2b), although few abnormally grown grains are also present. An abnormally grown grain in this sample is highlighted in the enclosed area in Fig. 2b. A much more homogeneous grain size distribution with profuse Σ3 boundaries is observed in sample H (Fig. 3a). It is to be noted here that samples G and I have similar microstructure. The enclosed area in Fig. 3a is magnified and shown in Fig. 3b to highlight the significant number of Σ3-Σ3-Σ9 and Σ3-Σ9-Σ27 triple junctions (marked by white circles in Fig. 3b) that are present in this sample. As a consequence, majority of Σ3 boundaries are an integral part of the grain boundary network. Further, due to the presence of such high fractions of $\Sigma 3^n$ triple junctions, the random HABs connectivity has been significantly disrupted (Fig. 3c).

The GBCD data in terms of $\Sigma 3^n$ boundaries for all the OTMP samples is shown in Fig. 4. The fraction of Σ3 boundaries is shown in Fig. 4a, while the Σ9 and Σ27 fractions are shown in Fig. 4b. It is seen from the Fig. 4a that the fraction of Σ3 boundaries has increased in all thermo-mechanically processed samples when compared to the SA sample. However, the improvement in Σ3 fraction is significant in samples E to I. A significant increase in Σ9 and Σ27 fractions is also observed in these samples (Fig. 4b). The average grain size (with and without twin[1]) in each processing condition is shown in Fig. 4a. The average grain size shows a trend similar to that of Σ3 boundaries (Fig. 4a). The average grain size in sample H, in which ~70% of $\Sigma 3^n$ boundaries was obtained, is 47 μm (without twins) and 12 μm (with twins) as compared to 18 μm (without twins) and 9 μm (with twins) in SA sample. This reveals that a very high fraction of $\Sigma 3^n$ has been achieved with moderate increase in average grain size. The hardness[2] in this condition (sample H) is 126 ± 3 HV as compared to 140 ± 4 HV in SA specimen. This indicates that GBE microstructure has been realized only at the cost of marginal (~10%) reduction in strength.

In order to understand the influence of "strain–temperature–time" relationship during OTMP in alloy D9, kernel average misorientation (KAM)[3] maps of samples B and H are evaluated and shown in Fig. 5. It is to be noted here that sample B represents the processing condition in which the increase in $\Sigma 3^n$ is marginal, whereas sample H shows profuse multiple twinning. The KAM map can be used to evaluate localized plastic strain in materials [31]. The higher KAM values in the grains correspond to higher local misorientations (i.e., higher local stored energies) and vice versa. It can be observed that the larger grains in sample B (Fig. 5a) have lower KAM. This indicates that these grains with lower KAM have grown predominantly at the expense of those with higher KAM. Sample H, on the other hand, shows very low KAM in all the grains (Fig. 5b).

The GBCD data in terms of $\Sigma 3^n$ boundaries for ITMP samples is shown in Fig. 6. The fraction of Σ3 boundaries

[1] The twin boundaries that were excluded in the calculation of average grain size were Σ3 and Σ9 boundaries within a tolerance of 5°.

[2] The hardness was measured with a FIE VM 50 Vickers hardness tester with 5 kg load for 15 s dwell time.

[3] The color-scale-coded KAM map is plotted on the basis of first-neighbor kernel parameter with a maximum misorientation angle of 5°.

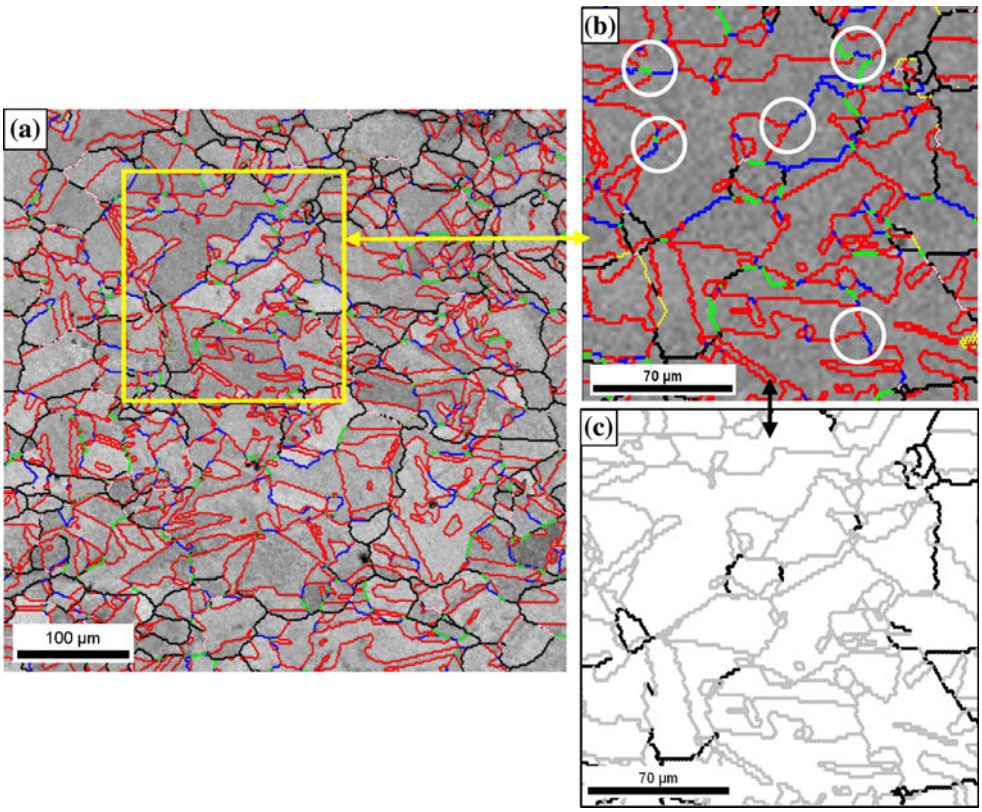

Fig. 3 **a** IQ map of specimen H. Color code convention is same as in Fig. 2; **b** Enclosed section of (**a**) at a higher magnification to show multiple twinning; **c** The grain boundary reconstructed map of the same location in which $\Sigma 3^n$ boundaries are shown in *gray* color while other boundaries are shown in *thick black line* to assess the connectivity

is shown in Fig. 6a, while the Σ9 and Σ27 fractions are shown in Fig. 6b. It is seen that the proportion of Σ3s is always higher after multiple iterations when compared to the SA condition. The Σ3 fraction increases to 62% after 2nd iteration (sample GG) as compared to 56% in 1st iteration (sample G). A slight drop in Σ3 fraction is observed after 3rd iteration (sample GGG). However, Σ3s increase again after 4th iterations (sample GGGG) and become comparable to that of 2nd iteration. The fraction of Σ9 and Σ27, on the other hand, decreases in the 2nd, 3rd and 4th iteration as compared to 1st iteration (Fig. 6b). This drop in Σ9 and Σ27 is more perceptible after 3rd iteration (sample GGG). Figure 7 shows the typical microstructural evolution after 2nd iteration. It could be observed that the topological appearance of the microstructure is similar to that of sample H (Fig. 3a). A similar microstructural evolution has also been observed after 3rd and 4th iteration. The enclosed area in Fig. 7a is enlarged (Fig. 7b) to show that significant number of Σ3-Σ3-Σ9 or Σ3-Σ9-Σ27 triple junctions (highlighted by white circles in Fig. 7b) exist in this sample. As a consequence, the random HABs connectivity in this specimen has been significantly disrupted (Fig. 7c).

Figure 8 illustrates the deviation of Σ3 and Σ9 boundaries from the ideal orientation in both the OTMP and ITMP specimens. It could be observed that majority of Σ3 and Σ9 boundaries in the SA samples are within 2° from the ideal orientation. A larger deviation in Σ3 and Σ9 boundaries from their exact misorientations is observed in sample B (Fig. 8a). However, these boundaries are more closely aligned (within 1.5°) towards the ideal orientation in samples G and H (Fig. 8a, b). Almost similar profiles were observed in all the iterative thermo-mechanically processed specimens (Fig. 8b).

Discussion

One-step processing

It was observed in the present study that Σ3 fraction increases significantly in OTMP samples E to I (see Fig. 4). The increase in Σ3 boundaries could be attributed to the formation of new Σ3 boundaries by geometrical interaction between pre-existing Σ3 boundaries (i.e., multiple twinning) and/or formation of new twins during annealing following cold deformation. According to the CSL rule, interaction between two Σ3 boundaries may form a Σ9 boundary according to the relationship $\Sigma 3 + \Sigma 3 = \Sigma 9$ [32]. When a Σ9 boundary generated in this way encounters another Σ3 boundary, it results in either a new Σ3 boundary based on the relationship $\Sigma 3 + \Sigma 9 = \Sigma 3$, or a Σ27 boundary following the relationship $\Sigma 3 + \Sigma 9 = \Sigma 27$. However, a look at the statistics of the Σ3, Σ9, and Σ27 boundaries (see Fig. 4) reveals that the increase in number

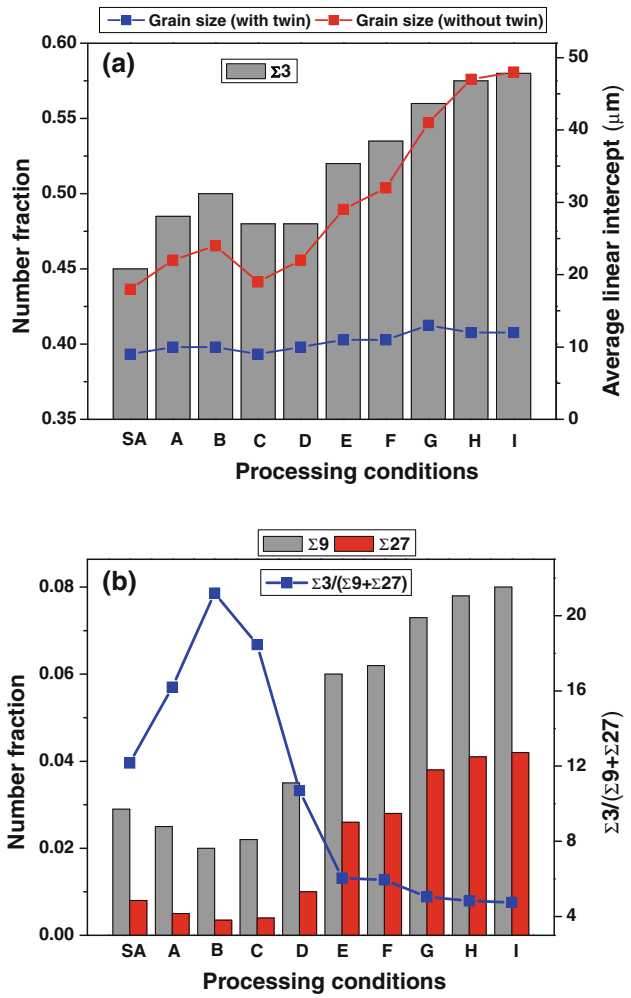

Fig. 4 Frequency distributions of **a** Σ3 boundaries [average grain size (with and without twins) in each condition is also indicated]; **b** Σ9 and Σ27 boundaries [(Σ3/Σ9 + Σ27) is also shown to assess random boundary connectivity] in one-step thermo-mechanically processed specimens

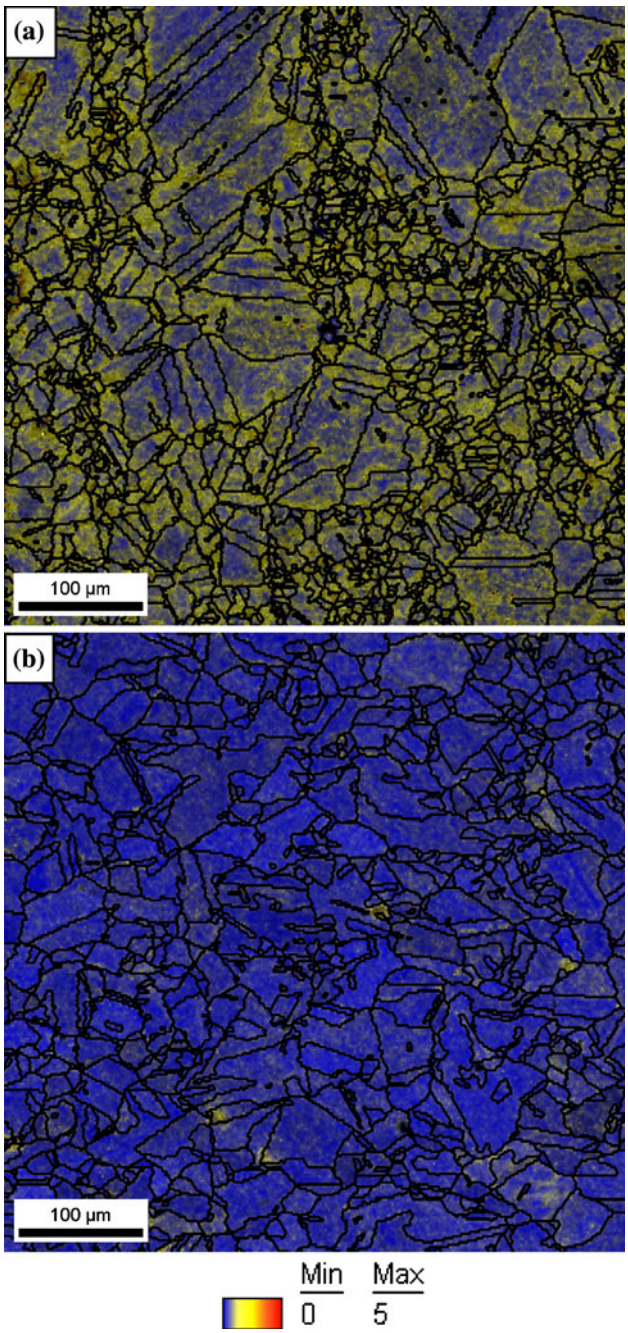

Fig. 5 Color-scale-coded kernel average misorientation (KAM) map of samples **a** B; and **b** H

fraction of Σ3 boundaries is much more than that of Σ9 or Σ27 boundaries. For example, the number fractions of Σ3 boundaries have increased from 0.45 in SA condition to 0.58 in specimen I. Whereas, number fraction of Σ9 and Σ27 boundaries have increased from 0.029 and 0.008 in SA condition to 0.08 and 0.042 in specimen I. This signifies that $\Sigma3 + \Sigma9 = \Sigma3$ event occurs more frequently than the $\Sigma3 + \Sigma9 = \Sigma27$ event. This has also been categorized as "Σ3 regeneration mechanism", which states that $\Sigma3^n + \Sigma3^{n+1} = \Sigma3$ occurs predominantly at triple junctions than $\Sigma3^n + \Sigma3^{n+1} = \Sigma3^{n+2}$ [33, 34]. It may be noted that though recently Reed et al. [35, 36] questioned the validity of Σ3 regeneration model and propose an alternative model, the Σ3 regeneration processes are not completely ruled out and are likely to occur within a twin related domain (TRD) [36]. However, this aspect needs to be looked into through an in-depth study.

As effective disruption of random boundary connectivity occurs with the introduction of Σ3–Σ3–Σ9 and Σ3–Σ9–Σ27 triple junctions, the ratio of Σ3 to (Σ9 + Σ27) would provide better indication of the fragmentation of random HABs network. In this context, Σ9s are key elements for GBE as they act as bridging segments between Σ3 boundaries [19]. The ratio of Σ3 to (Σ9 + Σ27) for one-step thermo-mechanically processed samples is shown in Fig. 4b. A higher ratio in samples A to D indicates that

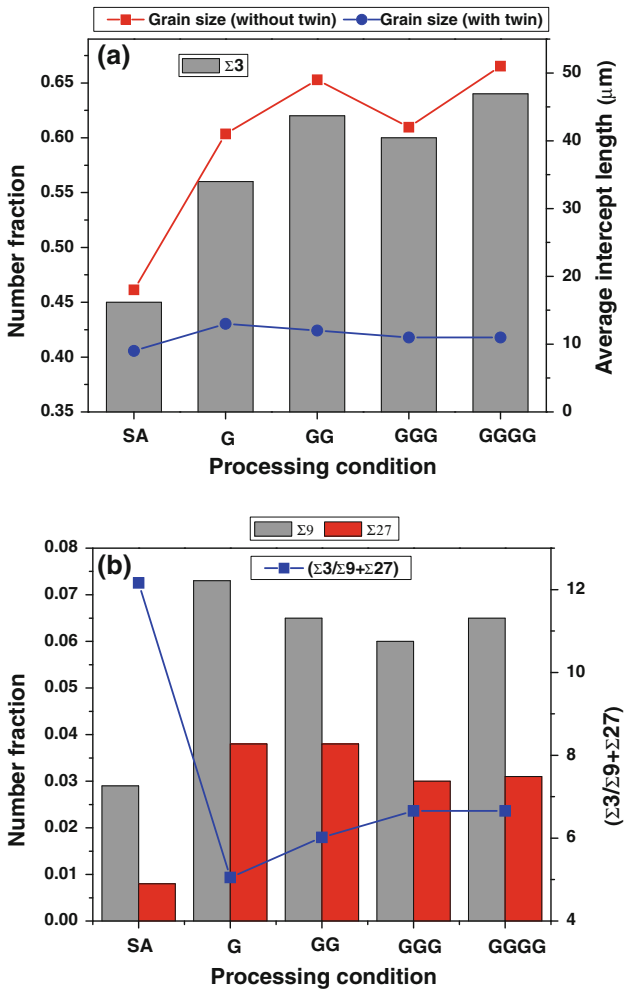

Fig. 6 Frequency distributions of **a** Σ3 boundaries [average grain size (with and without twins) in each condition is also indicated]; **b** Σ9 and Σ27 boundaries [(Σ3/Σ9 + Σ27) is also shown to assess random boundary connectivity] in iterative thermo-mechanically processed specimens

substantial amount of random HABs clusters with significant connectivity exist in these samples. This is also evident from the EBSD reconstructed grain boundary map of the sample B (Fig. 9a). Samples E to I, on the other hand, exhibit profound multiple twinning as revealed by the lower Σ3 to (Σ9 + Σ27) ratio (Fig. 4b). Consequently, a significant disruption of random HABs connectivity is observed due to the direct incorporation of Σ3 and its variants (Fig. 9b).

The understanding of the reasons for the prolific multiple twinning observed in the samples E to I would help to unravel the underlying mechanism associated with low-strain GBE processing. It has been shown by a TEM study that lower level of deformation (~10%) is insufficient to trigger recrystallization [37]. Rather, strain-induced boundary migration (SIBM) due to local variation in stored energy occurs if the thermal driving force (i.e., annealing temperature and time) is sufficient. During SIBM, migrating high-angle grain boundaries eliminate lattice dislocations. In the course of such grain boundary migration, multiple twinning occurs provided the grain boundary moves at an intermediate velocity that is suitable for twin nucleation and multiplication [19, 20]. The higher KAM in the smaller grains in sample B (Fig. 5a) indicates the presence of retained strain. This signifies that a combination of annealing temperature and time is not sufficient to promote SIBM in this sample. Rather, grains with lower KAM have grown predominantly at the expense of those with higher KAM. This is due to the fact that grains with lower KAM (i.e., with lower stored energy) have an energy advantage to consume their neighboring grains with higher KAM [29]. Due to such preferential growth of a few grains, the final microstructure contains a combination of very large and very small grains (Fig. 2a). Since, only few grains grew rapidly, interactions between pre-existing Σ3s are limited in this sample. This is also confirmed by a marginal increase in Σ9 and Σ27 boundaries (Fig. 4b). Due to the limited interaction between Σ3s, the regenerated Σ3 boundaries are fewer. The moderate increase in Σ3 boundaries (Fig. 4a) is primarily due to formation of new annealing twins during grain growth. As suggested by Gleiter [38], annealing twins usually nucleate in front of moving grain boundaries by "growth accidents". It may be noted here that almost similar GBCD and microstructural appearance (i.e., anomalous grain growth) was observed in our recent study [29] when alloy D9 specimens were subjected to annealing in the temperature range 1,173–1,273 K up to 2 h with and without 5% prior deformation. On the other hand, the "strain–temperature–time" response in sample H is markedly different. The very low KAM in all the grains in sample H (Fig. 5b) indicates the absence of retained strain. It is apparent that the combination of deformation and thermal activation energy is sufficient to promote SIBM in this sample, which in turn eliminates the strain. During such grain boundary migration, interactions between pre-existing Σ3 boundaries occur resulting in multiple twinning and this contributes to the increase in fraction of $\Sigma 3^n$ boundaries.

Iterative processing

The evolution of $\Sigma 3^n$ boundary fraction during ITMP was found to fluctuate. While the Σ3 fraction increased after 2nd and 4th iteration, a noticeable drop is observed after 3rd iteration (Fig. 6a). Fluctuations in the Σ3 fraction during the iterative processing have also been reported in earlier studies [16, 19, 20, 39, 40] and this is often explained in terms of accumulation of strain in the microstructure during initial iterations. Although random HABs act as a sink for dislocations during annealing,

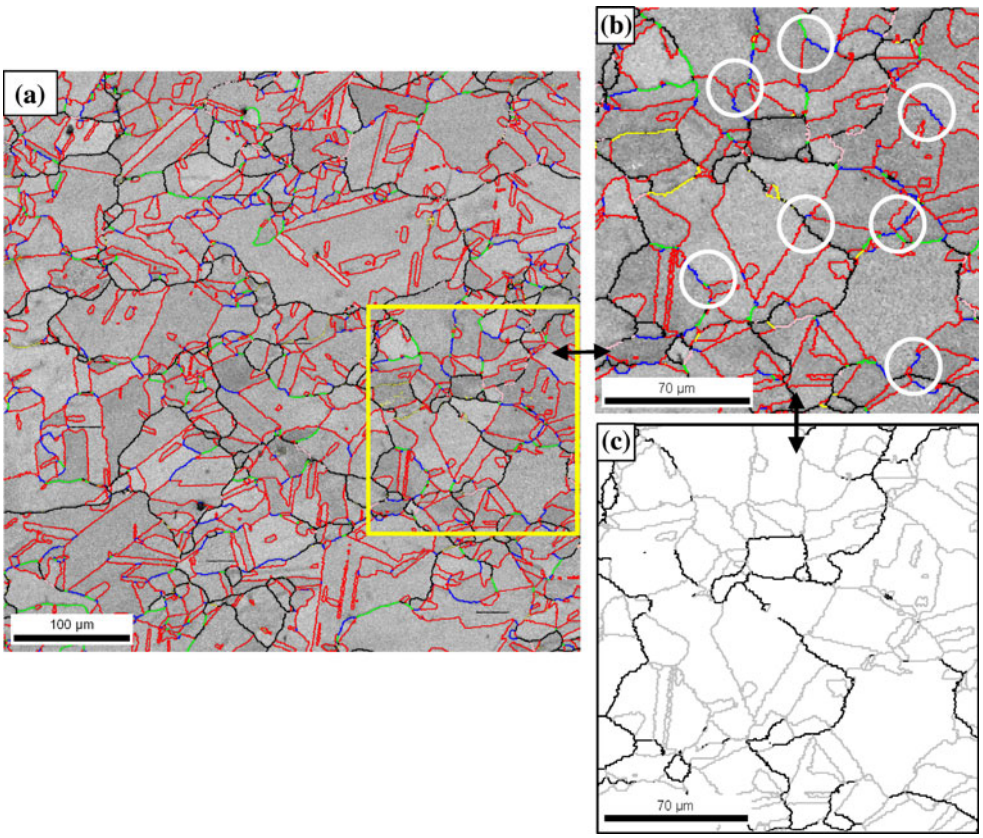

Fig. 7 IQ map of samples **a** GG Color code convention same as in Fig. 2; **b** Enclosed section of (**a**) at a higher magnification to show multiple twinning; **c** The grain boundary reconstructed map of the same location in which $\Sigma 3^n$ boundaries are shown in *gray* color while other boundaries are shown in *thick black line* to assess the connectivity

boundaries like Σ3s have lower dislocation annihilation rate since they have a periodic structure [41]. Hence, extrinsic dislocations have a propensity to be pinned in pre-existing dislocation arrays in Σ3 boundaries [41]. During the early iterations (1st and 2nd), strain is thereby accumulated due to dislocation pile-up at twin boundaries and this increases the internal stress and the driving force for boundary migration. As a consequence, there is now an increased driving force for grain boundary migration during subsequent strain increments. As a result, during 3rd iteration, mobile boundaries (particularly incoherent Σ3s and Σ9s) move very rapidly through the microstructure and sometimes annihilate few twins [42]. During the 4th iteration, there is now less stored strain in lattice and hence less driving force for grain boundary migration. The boundaries move more slowly, at an intermediate velocity which is optimal for the nucleation and generation of annealing twins. It may be noted that the aggregated proportions of $\Sigma 3^n$ ($n > 1$) boundaries do not build up in the microstructure through 2nd, 3rd, and 4th iterations (Fig. 6b). This is because Σ9 and Σ27 boundaries are removed by the back twinning mechanism as suggested in "Σ3 regeneration model". As a result of this, new Σ3 boundaries are replenished in the microstructure [40]. This also needs to be looked into in the light of an alternative view point [36].

In addition to proportion of $\Sigma 3^n$ boundaries, deviation of these boundaries from their ideal Σ misorientation is also an important parameter. Loss of twin orientation in sample B (Fig. 8a) is due to the deviation of pre-existing twin boundaries from the allowable limit due to imposed strain. Presence of imposed strain in lattice, particularly in smaller grains is evident in sample B (see Fig. 5a). Absence of retained strain at higher annealing temperature (Fig. 5b) allows Σ3 and Σ9 boundaries to orient themselves towards minimum energy positions. Although strain seems to be accumulated at twin boundaries due to dislocation pile-up during early iterations in the ITMP specimens, it is insufficient to change the orientation of the Σ3 and Σ9 boundaries (see Fig. 8b).

The present study established (through KAM analysis of GBE and non-GBE microstructures) that there exist optimum combinations of cold deformation, annealing temperature, annealing time, and numbers of iteration for achieving multiple twinning by SIBM that eventually increases the proportion of Σ3 boundaries and its variants and breaks down the random connectivity of HABs. The highest fraction of $\Sigma 3^n$ boundaries with minimum deviation from exact misorientation has been achieved in alloy D9 through a two and four step ITMP comprising of 10% deformation followed by annealing at 1,273 K for 0.5 h. The two step iterative processing is more attractive for

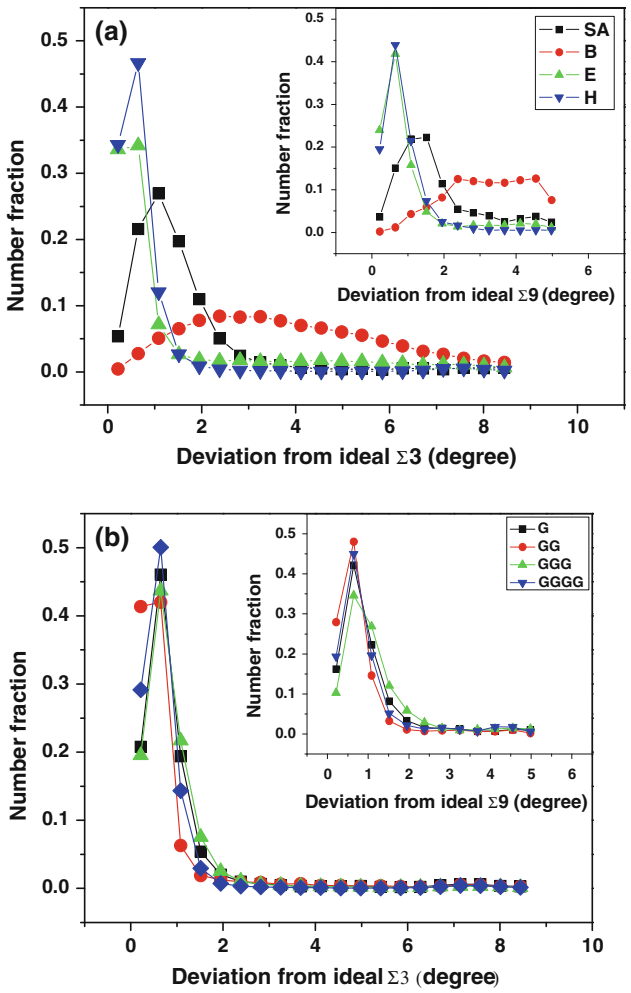

Fig. 8 Deviation of Σ3 and Σ9 boundaries from its ideal orientation in samples **a** SA, B, E, and H; **b** ITMP specimens

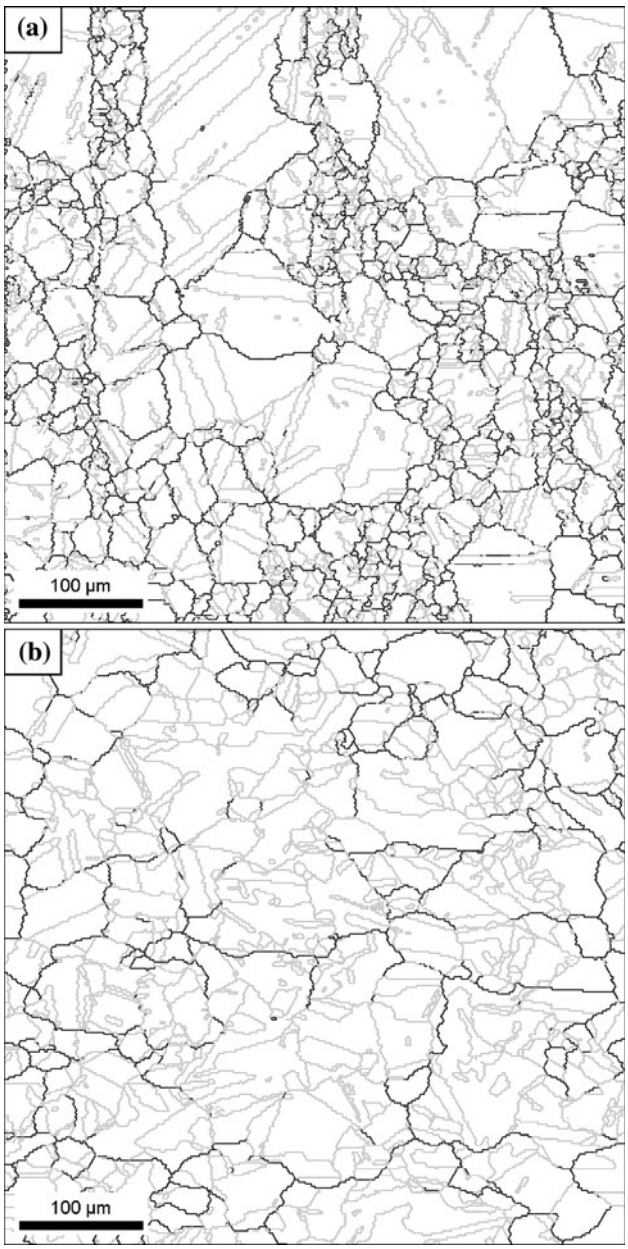

Fig. 9 Grain boundary reconstruction from EBSD data for sample **a** B; and **b** H (*thick black* and *thin gray lines* represent random HABs and low Σ CSL boundaries, respectively)

industrial application due to lower processing cost. A significant disruption in random HABs connectivity has also been achieved in this condition due to presence of large number of Σ3-Σ3-Σ9 and Σ3-Σ9-Σ27 triple junctions. Such modifications in microstructure are expected to result in improved grain boundary properties.

Conclusions

One-step and iterative thermo-mechanical processing has been carried out to enhance $\Sigma 3^n$ boundaries in a Ti-modified austenitic stainless steel (alloy D9). Based on this study, following conclusions are arrived at:

1. A one step thermo-mechanical processing comprising of 10% thickness reduction followed by annealing at 1,173 K for 0.5–2 h was found to induce anomalous grain growth with moderate increase in $\Sigma 3^n$ boundaries. The moderate increase in Σ3 boundaries is primarily due to formation of new annealing twins during grain growth. A substantial amount of random HABs clusters with significant grain boundary connectivity existed in these processing conditions.
2. Prolific multiple twinning with minimum deviation of Σ3 and Σ9 boundaries from their exact misorientation was obtained after annealing at 1,273 K for 0.5–2 h. Significant disruption in random HABs was achieved in this condition due to the presence of large number of Σ3-Σ3-Σ9 or Σ3-Σ9-Σ27 triple junctions that were generated via multiple twinning. A high fraction of $\Sigma 3^n$ boundaries (~67–70%) was achieved in these

processing conditions with moderate increase in the average grain size estimated without considering twin boundaries as grain boundaries.

3. Based on the outcome of the one-step processing, iterative processing (up to 4 cycles) was carried out on SA specimens employing 10% thickness reduction followed by annealing at 1,273 K for 0.5 h. The evolution of $\Sigma 3$ boundaries during ITMP was found to be fluctuating. While the fraction of $\Sigma 3$ boundaries increased after 2nd and 4th iteration, a perceptible drop was observed after 3rd iteration. This was attributed to the increased driving force for grain boundary migration due to dislocation pile-up at twin boundaries during initial iterations. After second iteration, the fraction of $\Sigma 3^n$ boundaries ($\sim$73%) is higher than those obtained after one step processing.
4. A two step ITMP comprising of 10% deformation followed by annealing at 1,273 K for 0.5 h is the recommended thermo-mechanical processing treatment to produce GBE microstructure in alloy D9.

Acknowledgements The authors are thankful to Dr. Satyam Suwas, Department of Materials Engineering, IISc Bangalore, India, for extending the rolling mill facility during this study. Thanks are also due to Mr. Nilesh Gurao, Department of Materials Engineering, IISc Bangalore, for his help during rolling. One of the authors (VSS) thanks the Indo-US Science and Technology Forum (IUSSTF) for a sabbatical research fellowship during the period this article was finalized.

References

1. Watanabe T (1984) Res Mech 11:47
2. Li C, Williams DB (2005) Phil Mag 85:2023
3. Krupp U (2008) J Mater Sci 43:3908. doi:10.1007/s10853-007-2363-6
4. Bechtle S, Kumar M, Somerday BP, Launey ME, Ritchie RO (2009) Acta Mater 57:4148
5. Kokawa H (2005) J Mater Sci 40:927. doi:10.1007/s10853-005-6511-6
6. Tan L, Sridharan K, Allen TR, Nanstad RK, McClintock DA (2008) J Nucl Mater 374:270
7. Jones R, Randle V (2010) Mater Sci Eng 527:4275
8. Kokawa H, Shimada M, Michiuchi M, Wang ZJ, Sato YS (2007) Acta Mater 55:5401
9. Watanabe T (1993) Mater Sci Eng A 166:11
10. Kobayashi S, Inomata T, Kobayashi H, Tsurekawa S, Watanabe T (2008) J Mater Sci 43:3792. doi:10.1007/s10853-007-2236-z
11. Watanabe T, Tsurekawa S, Kobayashi S, Yamaura S (2005) Mater Sci Eng A 410–411:140
12. Reed BW, Kumar M, Minich RW, Rudd RE (2008) Acta Mater 56:3278
13. Lejcek P, Hofmann S, Paidar V (2003) Acta Mater 51:3951
14. Saylor DM, El-Dasher BS, Rollett AD, Rohrer GS (2004) Acta Mater 52:3649
15. Kim CS, Hu Y, Rohrer GS, Randle V (2005) Scripta Mater 52:633
16. Coleman M, Randle V (2008) Metall Mater Trans A 39:2175
17. Rohrer GS, Randle V, Kim CS, Hu Y (2006) Acta Mater 54:4489
18. Randle V, Jones R (2009) Mater Sci Eng A 524:134
19. Owen G, Randle V (2006) Scripta Mater 55:959
20. Wang W, Guo H (2007) Mater Sci Eng A 445–446:155
21. Chowdhury SG, Kumar P, Das A, Das SK, Mahato B, De PK (2008) Phil Mag Lett 88:407
22. Randle V (2004) Acta Mater 52:4067
23. Michiuchi M, Kokawa H, Wang ZJ, Sato YS, Sakai K (2006) Acta Mater 54:5179
24. Fang X, Zhang K, Guo H, Wang W, Zhou B (2008) Mater Sci Eng A 487:7
25. Chowdhury SG, Singh R (2008) Scripta Mater 58:1102
26. Singh R, Chowdhury SG, Chattoraj I (2008) Metall Mater Trans A 39:2504
27. Engelberg DL, Humphreys FJ, Marrow TJ (2008) J Microsc 230:435
28. Engelberg DL, Newman RC, Marrowa TJ (2008) Scripta Mater 59:554
29. Mandal S, Bhaduri AK, Sarma VS (2009) Mater Sci Eng A 515:134
30. Brandon DG (1966) Acta Metall 14:1479–1484
31. Jorge-Badiola D, Iza-Mendia A, Gutierrez I (2007) J Microsc 228:373
32. Lim LC, Raj R (1984) Acta Metall 32:1177
33. Randle V, Owen G (2006) Acta Mater 54:1777
34. Randle V (1999) Acta Mater 47:4187
35. Reed BW, Minich RW, Rudd RE, Kumar M (2004) Acta Cryst A60:263
36. Reed BW, Kumar M (2006) Scripta Mater 54:1029
37. Kumar M, Schwartz AJ, King WE (2002) Acta Mater 50:2599
38. Gleiter H (1969) Acta Metall 17:1421
39. Randle V, Coleman M (2009) Acta Mater 57:3410
40. Randle V, Davies H (2002) Metall Mater Trans A 33:1853
41. King AH (1985) Scripta Metall 19:1517
42. Randle V (2010) Mater Sci Technol 26:253